INSTITUTE OF PHYSICS PUBLISHING PLASMA PHYSICS AND CONTROLLED FUSION

Plasma Phys. Control. Fusion **47** (2005) L31–L40 doi:10.1088/0741-3335/47/9/L01

LETTER TO THE EDITOR

Alfvén eigenmode observations on DIII-D via two-colour CO_2 interferometry

M A Van Zeeland[1,2], G J Kramer[3], R Nazikian[3], H L Berk[4], T N Carlstrom[2] and W M Solomon[3]

[1] ORISE, PO Box 117, Oak Ridge, TN 37831-0117, USA
[2] General Atomics, PO Box 85608, San Diego, CA 92186-9784, USA
[3] Princeton Plasma Physics Lab., PO Box 451, Princeton, NJ 08543, USA
[4] Institute of Fusion Studies, University of Texas at Austin, Austin, TX 78712, USA

Received 6 May 2005, in final form 15 July 2005
Published 16 August 2005
Online at stacks.iop.org/PPCF/47/L31

Abstract

Measurements are presented of toroidicity-induced (TAEs) and reverse shear (RSAEs) Alfvén eigenmodes made using the standard two-colour CO_2 interferometer on DIII-D modified for increased bandwidth. Typical values of the effective line-integrated density perturbation in DIII-D are found to be $d(nL)/nL \sim 10^{-3}$, and comparisons are made with NOVA calculations as well as magnetic measurements. There is a strong difference in the measured power spectrum between vertical and radial chords through the plasma. On average, vertical views are characterized by a larger line-integrated density perturbation due to TAEs than radial chords. Radial chords, however, can be used much more reliably than vertical chords to identify the presence of RSAEs in the plasma—a result found to be due to the radially localized nature of these modes. In general, the apparent amplitude of the observed modes for both TAE and RSAE is found to be highly dependent on viewing location.

(Some figures in this article are in colour only in the electronic version)

1. Introduction

Toroidicity-induced Alfvén eigenmodes (TAEs) are fast-ion driven instabilities that, when strong enough, have been shown to cause undesirable losses of energetic particles in tokamaks [1, 2]. For next-step devices such as ITER, alpha particle driven TAE instability is predicted and there is a concern that substantial loss of hot fusion born alpha particles can then occur [3, 4]. Understanding the spatial structure and stability properties of TAEs through modelling and direct experimental observation is essential in order to have confidence in our ability to predict Alfvénic activity and their nonlinear consequences in future devices. In fact, a core diagnostic for TAEs has been identified as an essential need in ITER [5]. Such a measurement in burning plasma experiments is particularly difficult due to the large size scales

as well as the incredibly harsh environment. Previous diagnostics used in the investigation of Alfvén eigenmodes (AEs) include microwave reflectometry, beam-emission spectroscopy, soft x-ray emission imaging, beam-ion loss measurements, magnetic probes and more recently, microwave interferometry and far-infrared scattering [2, 6–8]. Magnetic probes are perhaps the most relied upon in present-day experiments; however, extrapolation of this method to ITER remains questionable due to the required separation of the probes from the plasma which leads to even poorer coupling between the wave excitation region and the detector than in present-day experiments. In fact, recent experiments have demonstrated that magnetic probes are not as efficient as some of the other techniques mentioned above in diagnosing core Alfvén activity [7].

The measurement of plasma density fluctuations by forward scattering of CO_2 radiation is a well-established technique [9]. Along these lines, measurements of plasma line-integrated density in tokamaks using two-colour vibration compensated CO_2 interferometers have become standard. Indeed the interferometer can be thought of as a far-forward scattering diagnostic of very low-k fluctuations. The scattered spectrum is an integral of all long wavelength fluctuations with wave vectors smaller than $2/a_0$ where a_0 is the Gaussian beam waist of the CO_2 beam. The use of short wavelength CO_2 radiation (10.6 μm) as opposed to microwaves becomes necessary due to refraction and rapid fringe shifts associated with high-density tokamak discharges. An additional requirement for ITER is a two-colour interferometer polarimeter for which CO_2 wavelengths are favoured. Such an interferometer would fulfil two separate diagnostic needs in ITER: a line-integrated density measurement as well as a core diagnostic of TAEs and other instabilities with a finite density perturbation.

This letter shows that a standard multi-chord, two-colour, vibration compensated CO_2 interferometer, regularly used for density feedback control of a tokamak plasma, is also capable of providing detailed information about the internal mode structure of AEs through their finite effective line-density perturbation. Typical line-integrated values of this density perturbation in DIII-D are found to be $d(nL)/nL \sim 10^{-3}$ or, depending on plasma density, approximately $O(10^{13})\,\mathrm{cm}^{-2}$. Additionally, comparisons are made with NOVA calculations as well as with magnetic measurements. There is a strong difference in the power spectrum between vertical and radial chords through the plasma measured with the CO_2 interferometer. The vertical views preferentially see TAEs and the pure radial view dominantly sees reverse shear Alfvén eigenmodes (RSAEs)/Alfvén Cascade mode [7, 8].

2. Diagnostic and observation

The real-time, two-colour, heterodyne interferometer system on DIII-D has been used extensively over the last 15 years for line-averaged density measurements and feedback control [10]. On DIII-D, several of the interferometer optical components are mounted directly on the vessel, which during a shot can vibrate with amplitudes as large as 1 mm. At the CO_2 wavelength used, this amounts to approximately 100× the phase shift resulting from the plasma in a typical DIII-D discharge. Therefore, in order to separate plasma induced phase shift from vibration induced phase shift, each of the four chords utilizes a 10.6 μm CO_2 laser (<8 W) and either a 0.632 or a 3.39 μm HeNe laser (1 cm diameter beam) for vibration compensation. This technique is described in detail elsewhere and will not be reviewed here except to say that the phase shift due to plasma alone can be approximated by the line-integral along the laser path, $\phi_{\mathrm{plasma}} = \lambda r_e \int n_e \, dl$, where λ is the probing wavelength, n_e is the electron density and $r_e = 2.82 \times 10^{-13}$ m (the classical electron radius) [10, 11]. The current system employs a combination of analog and digital circuitry in order to provide 'real-time' line-density measurements with a bandwidth of <40 kHz [10]. In principle, the bandwidth of the heterodyne two-colour system on DIII-D has been limited at 3 levels: (1) the CO_2 detectors <100 MHz,

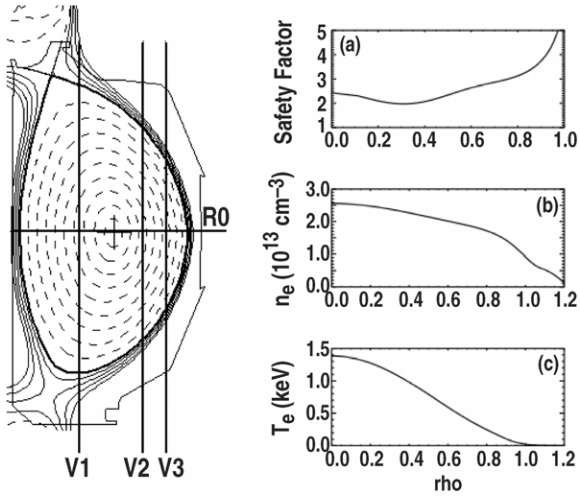

Figure 1. Discharge 120655, $t = 575$ ms, EFIT equilibrium reconstruction showing interferometer chords. The dashed contours are contours of constant poloidal magnetic flux. The right panels from top to bottom are: (*a*) safety factor, (*b*) electron density from Thomson scattering measurements and (*c*) electron temperature from Thomson scattering. The major radii of the vertical viewing interferometer chords are: V1 = 1.48 m, V2 = 1.94 m and V3 = 2.10 m. The magnetic axis is located at $R_m = 1.74$ and the toroidal field on-axis is $B_T = 1.24$ T.

(2) the 6 MHz wide bandpass filters around the 40 MHz intermediate frequency <6 MHz and (3) the real-time electronics and density calculation <40 kHz. By digitizing the outputs of each laser's quadrature phase detectors directly, and doing the density calculation at a later time, the bandwidth is then only limited to either 6 MHz or half of the digitization rate, whichever is lower. Additionally, this allows one to compensate in software for amplitude imbalances and dc offsets associated with the analog quadrature phase detectors, further increasing the accuracy of the system [11]. As a note, faster digitizers can be used in parallel with the old system so that the real-time aspect of the interferometer is preserved. Although the data presented in this paper were taken using a true two-colour interferometer, equivalent spectra have been obtained by using only the CO_2 phase signal and forgoing the vibration compensation. This, however, does not allow the investigation of lower frequency modes that can be complicated by vibrations in the system.

Shown in figure 1 is a plasma equilibrium magnetic flux reconstruction using EFIT with the overlayed interferometer chord positions [12]. Each chord is double pass and reflects off a corner cube located on top of the device for the vertical chords (V1, V2, V3) and on the inner wall for the radial chord (R0). The relevant profiles (q, n_e and T_e) are also shown.

Figure 2 shows windowed FFTs of fast interferometer data (*b*) and magnetic pickup loop data (*a*) for the discharge with the equilibrium plasma parameters shown in figure 1. The uncalibrated pickup loop is located inside the vacuum vessel at the outboard midplane. The magnetics shown in figure 2 are rich in structure with several different modes apparent. Within 100 ms after the turn-on time of the 2.5 MW, 78 kV neutral beam ($t = 300$ ms), TAEs of various poloidal (m) and toroidal (n) mode number starting around 100 kHz are destabilized and slowly decrease in frequency. Overlayed on the plot are the expected TAE frequencies in the lab frame for some of the modes, approximated by

$$f_{TAE} = \frac{V_A}{4\pi q R} + n f_\phi, \tag{1}$$

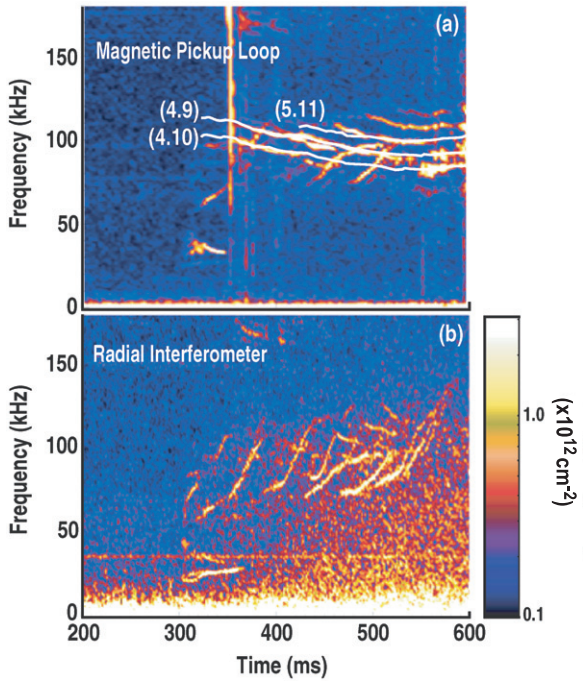

Figure 2. Windowed FFT for discharge 120655. 78 kV Neutral beam turn-on is at $t = 300$ ms. Log scale where white represents larger amplitude and a 1 kHz smoothing has been applied. (*a*) Uncalibrated magnetic pickup loop located inside the vacuum vessel at the outboard midplane. Overplotted white lines are the expected TAE frequencies for (n, m) from equation (1). (*b*) Radial fast interferometer chord, peak amplitude is 2.24×10^{12} cm^{-2}, corresponding to $d(nL)/nL \sim 10^{-4}$–10^{-3}, noise floor is O(10^{11} cm^{-2}).

where

$$q = \frac{2m + 1}{2n}. \tag{2}$$

R is the major radius, f_ϕ is the toroidal rotation frequency as inferred from additional diagnostic measurements and $V_A = B/(\mu_0 \rho_m)^{1/2}$ is the local Alfvén speed, with B the magnetic field and ρ_m the mass density. The injected neutral beam is sub-Alfvénic, $V_b/V_A = 0.71$ and $B_T = 1.25$ T. The toroidal mode numbers were identified via a best fit to the phase from an internal array of unequally spaced probes. In order to determine the temporal dependence of f_{TAE} for a given q, the local toroidal rotation and density must be included. Unfortunately, an accurate determination of the q-profile was not possible until $t = 575$ ms, when the motional Stark effect (MSE) diagnostic began its data acquisition. Instead, it was approximated by EFIT reconstruction using magnetic diagnostics alone, which was shown to agree with the MSE derived profile at $t = 575$ ms to within 10–20% depending on radius. At each timestep, f_{TAE} for a given q was obtained by first mapping q to a given flux surface and then obtaining the relevant parameters through fitted profiles. The toroidal rotation was obtained directly from charge exchange recombination (CER) measurements and was roughly $f_\phi = 1$–3 kHz and constant after $t = 350$ ms. Poloidal mode numbers were obtained by using the best fit of equation (1) to the data. The major purpose of the overplotted f_{TAE} lines is to convince the reader that these modes are indeed TAEs. In addition to TAEs, there is a hint of modes shifting up in frequency, which become much more apparent after $t = 440$ ms. These modes have

been identified as RSAEs that are also known as Alfvén cascades [13]. RSAEs are a class of AE that can be excited in the low shear region of a tokamak near the minimum of the magnetic safety factor when there is an inverted shear profile such as that shown in figure 1 or when there is an extremely weak central shear region [14–16].

In comparison, the radial interferometer view, shown in figure 2(*b*), is characterized by an almost complete lack of observable TAE activity with only a few of the higher harmonics visible for approximately 25–50 ms bursts. Despite the global nature of the TAE its spatial structure is such that the mode is not seen on the radial interferometer chord. This point will be addressed in more detail below where a favourable comparison of the data with NOVA calculations is made. In contrast, the upward chirping RSAEs are apparent on the radial chord. In fact, the RSAE is more clearly seen by the interferometer than with the magnetic probes. These measurements are consistent with data taken using a far-infrared (300 GHz) forward scattering system with a similar viewing geometry and wavenumber resolution [8]. RSAEs have been previously observed in JET using a microwave interferometer and in C-Mod by the phase contrast imaging system [7, 17, 18]. As described in other papers, the RSAE frequencies are intrinsically tied to the evolution of the minimum q in the plasma ($q_{\min}$) and have been used very successfully to determine the minimum rational q present in a plasma [13, 19, 20]. Integer and half-integer crossings of $q_{\min}$ are distinguished by a bunching of modes such as that observable near $t = 575$ ms. This is supported by the MSE derived q-profile shown in figure 1, which has an integer minimum $q = 2$ at $t = 575$ ms. Also visible on each diagnostic is a mode beginning around $t = 370$ ms near 175 kHz and one beginning a $t = 300$ ms near 30–40 kHz. CONT calculations of the Alfvén gap structure show that these may be an ellipticity induced Alfvén eigenmode (EAE), and beta induced Alfvén eigenmode (BAE), respectively [21].

Figure 3 shows windowed FFTs of interferometer data for discharges with similar AE activity to that of figure 2. Figure 3(*a*) is from the vertical interferometer chord on the high field side of the magnetic axis (V1) and figure 3(*b*) is from the radial chord. For this discharge the neutral beams come on at $t = 300$ ms, $V_b/V_A = 0.50$, $n_e(0) = 2 \times 10^{13}$ cm^{-3}, $T_e(0) = 1.1$ keV, $B_T = 1.8$ T. As with the previous figure, the radial chord shows the RSAE and not the TAE. Conversely, the TAE is observable on the vertical chord and possibly the RSAE but to a much lesser extent. This is not specific to the single vertical chord shown. In fact, the same qualitative observation is made by all three of the vertical chords, with the lower-field chords seeing the largest amplitude line-integrated fluctuations. The lack of RSAE activity on the vertical chords is assumed to be a result of the localization of the mode to regions of weak or reversed shear, the profile of which for these discharges is very similar to that of figure 1. Once the existence of an RSAE is established with the radial chord, this fact can be used to constrain the location of local minima of q and $q_{\min}$ itself to the inside of the minimum minor radius viewable by any vertical chord. Through comparison with the equilibrium reconstructions for these discharges, this constrains the mode and $q_{\min}$ to $\rho < 0.3$, in agreement with the location of $q_{\min}$ from MSE measurements ($q_{\min} < 0.26$).

Unfortunately, magnetic pickup loops were not available for the discharges shown in figure 3 so toroidal mode numbers could not be obtained as readily as those of figure 2. However, some information can be obtained by noting the peak amplitude modes' relative spacing. The lab frequencies corresponding to five clearly observable, nearly equally spaced modes at $t = 410$ ms in figure 3(*a*) were identified as $f_{TAE} = 112$, 122.5, 131, 140, 148 kHz. The average spacing of these modes is 9 kHz. The toroidal rotation for this discharge at $t = 410$ ms as obtained from CER measurements has an average value of roughly $f_\phi = 3$–4 kHz. To a rough approximation, the relative spacing can be obtained from simply $\Delta f = \Delta n f_\phi$, indicating that the observed toroidal mode numbers are not consecutive integers

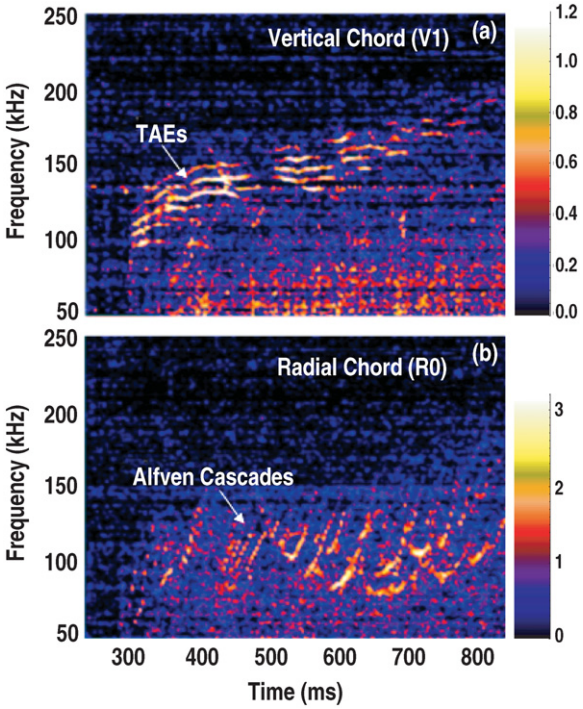

Figure 3. Windowed FFT of interferometer data, normalized amplitudes with white representing larger values—linear scale. (*a*) discharge 117745 vertical chord (V1), (*b*) discharge 117758 radial chord. A 2 kHz smoothing and the spectra at $t = 250$ ms has been subtracted off to reduce noise. Peak amplitude is 7.0×10^{11} cm^{-2}, corresponding to $d(nL)/nL \sim 10^{-4}$, noise floor is O(10^{11} cm^{-2}).

in contradiction to typical magnetic data commonly obtained in DIII-D [6]. This point will also be addressed in the next section.

3. NOVA analysis

In an attempt to gain a qualitative understanding of the interferometer measurements and to elucidate several subtle effects of the line-averaged measurement, NOVA calculations of TAEs with toroidal mode numbers ranging from $n = 2$–10 were carried out for discharge 117745, $t = 410$ ms. NOVA is a magnetohydrodynamic (MHD) code for tokamaks with energetic particles [22, 23]. As inputs, NOVA uses several geometrical factors as well as the experimentally measured radial profiles of: ion/electron density, toroidal rotation, safety factor, ion/electron temperature, $Z_{\rm eff}$ and pressure. Shown in figure 4(*a*) is the calculated oscillatory density perturbation for discharge 117745, $t = 410$ ms from an $n = 2$ TAE mode ($f = 94$ kHz). The right half of figure 4 shows the amplitude of the expected line-integrated density perturbation, $d(nL)$, for vertical (figure 4(*b*)) and horizontal (figure 4(*c*)) sightlines across the plasma as a function of major radius (vertical view) and vertical height (horizontal view). For reference, the actual experimental chord positions are shown in figure 1. For a given sightline, the fluctuating part of the line-integral oscillates in time at $f_{\rm TAE}$. The line-integrated density perturbation is then defined as the amplitude of this oscillatory density perturbation.

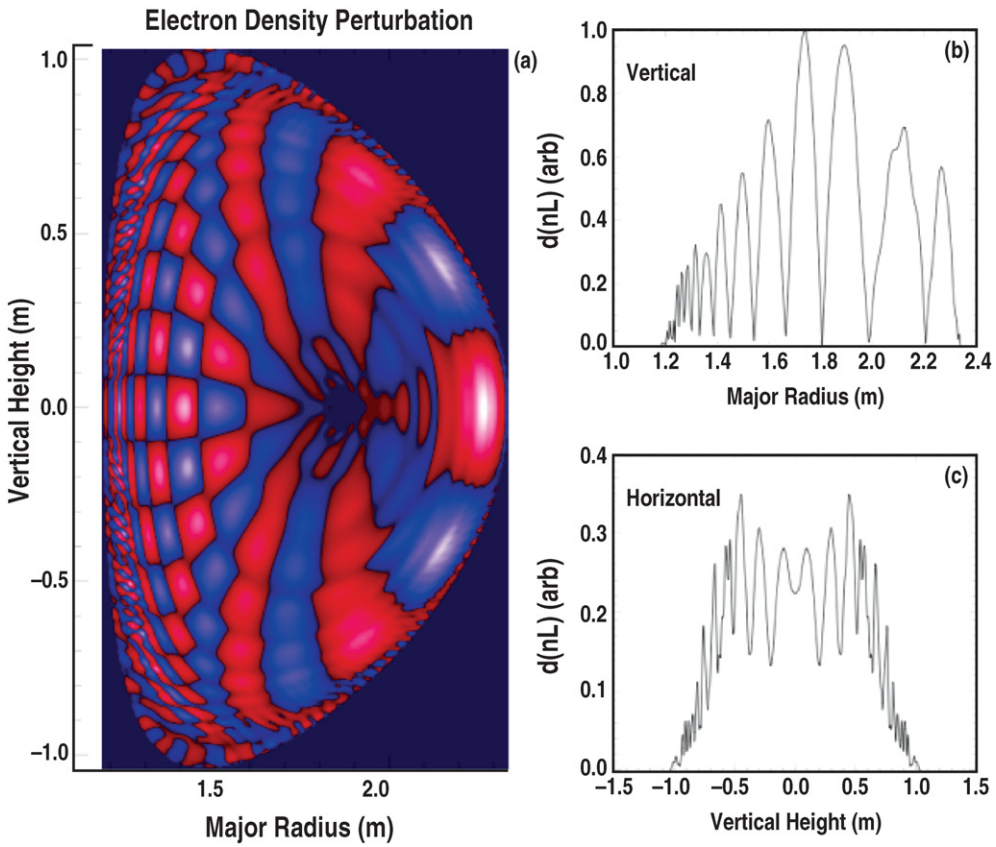

Figure 4. NOVA results for discharge 117745, $t = 410$ ms: (*a*) $n = 2$ electron density perturbation; (*b*) line-integrated density perturbation for a vertical view as a function of major radius and (*c*) line-integrated density perturbation for a horizontal view as a function of vertical height.

Several key features, some of which are verified by experimental observations, come out of the simulation analysis as follows:

1. In all cases, the peak line-integrated density perturbation as a function of major radius for vertical viewing chords is larger than that of the peak from a radial viewing chord at any vertical position. In fact, the average for $n = 2$–10 of the peak vertical/peak radial line-integrated density perturbation is roughly 4–5. This point is consistent with the data shown in figure 3. In figure 3, no TAEs were observed on the radial chord even though they were present in the plasma (as indicated by the V1 interferometer chord). Figure 2(*b*), however, shows that for large enough amplitudes, TAEs can be identified with the radial viewing interferometer as the simulation predicts. The TAEs become observable in figure 2(*b*) at approximately 475 ms and can be identified more clearly from a comparison with the magnetic probe data in figure 2(*a*). The observable modes correspond to the $(n, m) = (5, 11)$ and higher, and each is observable only for approximately 50 ms.

2. The vertical line-integrals are highly dependent on position and toroidal mode number creating a situation where for identical amplitudes, unlike magnetic probe data, it is not always possible to see consecutive mode numbers present in the plasma. For a given viewing radius and toroidal mode number, the line-integrated density perturbation may be close to zero, giving

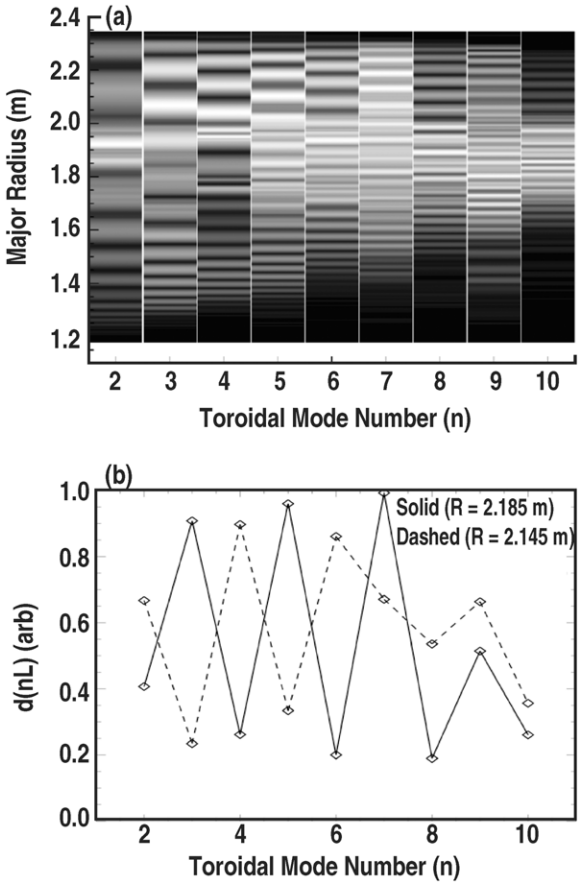

Figure 5. NOVA results for discharge 117745, $t = 410$ ms. (*a*) Vertical viewing line-integrated TAE density perturbation as a function of major radius and toroidal mode number. White corresponds to higher values, black to lower. (*b*) Line-plots derived from figure 5(*a*). Vertical view line-integrated density perturbation at two different major radii showing dependence on position and toroidal mode number. Solid and dashed curves at $R = 2.185$ m and $R = 2.145$ m, respectively.

the impression that the mode does not exist in the plasma, regardless of actual mode amplitude. Figure 4(*b*) conveys the strong dependence of the line-integrated density on the radial position for the $n = 2$ mode. Figure 5 is the generalization of figure 4(*b*) to all of the toroidal mode numbers investigated using NOVA generated data. It is the normalized sum of all of the vertical line-integrals for a given n as a function of major radius. White corresponds to higher values, black to lower. This figure conveys not only the strong dependence on the radial position of the vertical line integral amplitudes, but the strong dependence on toroidal mode number as well and, in general, to give the reader a glimpse of the very complex instrument function introduced by the interferometer with respect to TAE measurements. Figure 5(*a*) shows that as the vertical line-integral location moves radially the measured density perturbation appears very different for different n's even for identical mode amplitudes. This is depicted more clearly in figure 5(*b*), which is a direct comparison of two different major radii from figure 5(*a*). Figure 5(*b*) shows that at $R = 2.185$ m, $n = 3, 5, 7, \ldots$ appear much stronger than the even mode numbers, whereas at $R = 2.145$ m, $n = 2, 4, 6, \ldots$ are dominant. The same type of phenomena is true for radial viewing chord. This effect must be considered when interpreting line-averaged density

fluctuation measurements, especially if any comparison is being made of the relative density perturbation between different toroidal mode numbers. Possible experimental verification of the toroidal mode number dependence is shown in figure 3 which, as previously discussed, alludes to a non-consecutive spacing of toroidal mode numbers based on simple estimations using the measured toroidal rotation frequency Doppler shift.

3. For all simulation cases, the peak outboard ($R \geqslant R_{\mathrm{m}}$) line-integrated TAE density perturbations for vertically viewing chords are larger than that of the peak inboard views, where R_{m} refers to the magnetic axis. This result points to the ballooning nature of the TAE and is depicted in figure 4, which shows the line-integral amplitude peaking near the magnetic axis and the largest density perturbations on the outboard side. Through comparison of data obtained on V1, V2 and V3 there is some experimental indication of this phenomena.

4. In addition to the TAE, RSAEs were found using NOVA for discharge 117745. The calculated eigenmodes indeed showed strong localization to the region of zero shear, which for the shots shown was inside the minimum viewable radius of any interferometer chord. This explains the lack of RSAE activity on the vertical viewing chords and points to the possibility of obtaining information about the location of q_{min} as described previously. It should be pointed out that this does NOT mean that the RSAE cannot be seen on the vertical chords. Preliminary analysis of recent discharges with reverse shear have revealed core RSAE activity on the V2 interferometer chord.

For the CO_2 system described, all of these points are particularly important because the modes being observed are typically at most one–two orders of magnitude above the noise floor. For the various viewing geometries, this creates a situation where some modes are simply not discernable as with the radial view in figure 3 (where the TAEs are below the noise floor).

4. Conclusion

AEs have been observed in DIII-D using a standard two-colour vibration compensated CO_2 interferometer modified for increased bandwidth. Different viewing geometries exhibit very different spectra. TAEs are apparent on vertically viewing chords and to a lesser extent on the radial chord, while RSAEs are clearly seen on the radial chords but not on the vertical chords for the discharges that have been shown. For TAEs this difference has been explained by using results of NOVA eigenmode calculations, which show that there is a much larger line-integrated density perturbation for the vertical views than for the radial views. Additional features of the TAE observations have been confirmed by NOVA results, i.e. ballooning nature of TAEs and the possibility of a highly position dependent instrument function which can favour certain non-consecutively spaced toroidal mode numbers. This diagnostic technique has application in future burning plasma experiments in which a core diagnostic of TAEs is required to attempt to proactively limit fast-ion loss, as well as tokamaks in general, in which RSAEs are rapidly becoming a means of diagnosing information about the q-profile through Alfvén eigenmode spectroscopy. This study shows that with proper modelling, specific sightlines can be identified to maximize fluctuation signal levels from AEs.

This work was funded by the US Department of Energy under Cooperative Agreement No DE-FC02-04ER54698 and in part by an appointment to the US Department of Energy Fusion Energy Postdoctoral Research Program administered by the Oak Ridge Institute for Science and Education. Interesting and helpful discussions with Drs R L Boivin, J C DeBoo, W W Heidbrink, W A Peebles, T L Rhodes and E J Strait are greatly appreciated.

References

[1] Wong K L *et al* 1999 *Plasma Phys. Control. Fusion* **41** R1
[2] Carolipio E M *et al* 2001 *Phys. Plasmas* **8** 3391
[3] Gorelenkov N N *et al* 2003 *Nucl. Fusion* **43** 594
[4] Gorelenkov N N, Berk H L and Budny R V 2005 *Nucl. Fusion* **45** 226
[5] Boivin R L, Casper T A and Young K M 2004 *Plasma Phys. Control. Fusion* **46** A347
[6] Strait E J, Heidbrink W W and Turnbull A D 1994 *Plasma Phys. Control. Fusion* **36** 1211
[7] Sharapov S E *et al* 2004 *Phys. Rev. Lett.* **93** 165001-1
[8] Nazikian R M *et al* 2004 *Proc. 20th IAEA Fusion Energy Conf. (Vilamoura, Portugal, 2004)* http://www.cfn.ist.utl.pt/20IAEAConf/presentations.htm
[9] Slusher R E and Surko C M 1980 *Phys. Fluids* **23** 472
[10] Carlstrom T N, Ahlgren D R and Crosbie J 1988 *Rev. Sci. Instrum.* **61** 2865
[11] Van Zeeland M A and Carlstrom T N 2004 *Rev. Sci. Instrum.* **75** 3423
[12] Lao L L, St John H, Stambaugh R D, Kellman A G and Pfeiffer W 1985 *Nucl. Fusion* **25** 1611
[13] Sharapov S E *et al* 2001 *Phys. Lett.* A **289** 127
[14] Berk H L, Borba D N, Breizman B N, Pinches S D and Sharapov S E 2001 *Phys. Rev. Lett.* **87** 1085002
[15] Breizman B N *et al* 2003 *Phys. Plasmas* **10** 3649
[16] Kramer G J, Gorelenkov N N, Nazikian R M and Cheng C Z 2004 *Plasma Phys. Control. Fusion* **46** L23
[17] Nave M F *et al* 2004 *Rev. Sci. Instrum.* **75** 4274
[18] Snipes J A, Fasoli A, Bonoli P, Migliuolo S, Porkolab M, Rice J E, Takase Y and Wolfe S 2000 *Plasma Phys. Control. Fusion* **42** 381
[19] Sharapov S E *et al* 2001 *Phys. Plasmas* **9** 2027
[20] Joffrin E *et al* 2003 *Nucl. Fusion* **43** 1167
[21] Turnbull A D *et al* 1993 *Phys. Fluids* B **5** 2546
[22] Cheng C Z and Chance M S 1987 *J. Comput. Phys.* **71** 124
[23] Cheng C Z 1992 *Phys. Rep.* **211** 1